PROCEEDINGS, 51st Workshop on Geothermal Reservoir Engineering
Stanford University, Stanford, California, February 9-11, 2026
SGP-TR-230

Microseismic Plane Fitting at Utah FORGE Using a Bayesian Gaussian Mixture Model

[1]Nicholas Van Fleet, [1]Kristine L. Pankow, and [2]Dimitrios Karvounis

[1]Dept. of Geology and Geophysics, University of Utah, Salt Lake City, UT; [2]Geo-Energie Suisse, Zurich, Switzerland

Frederick Albert Sutton Building, 115 S 1460 E Room 211, Salt Lake City, UT 84112

nick.vanfleet@hotmail.com

Keywords: Utah FORGE, machine learning, microseismicity

ABSTRACT

The Utah Frontier Observatory for Research in Geothermal Energy (Utah FORGE) is a field scale laboratory near Milford, Utah designed to help de-risk enhanced geothermal systems (EGS). During EGS operations, pressurized fluids are injected to create a permeable reservoir. This process generates microseismicity. In 2024, stages 3R through 10 of the injection well were stimulated using both proppants and slick water. Microseismicity maps into two main fracture zones. This study establishes a workflow to characterize the internal nature of these fracture zones in order to better understand the risk potential of the fractures and to better inform future activities at the Utah FORGE site. Fractures are identified by clustering microseismic events using an unsupervised machine learning approach called Bayesian Gaussian Mixture Model (BGMM). BGMMs and the more popular K-Means clustering method are both unsupervised clustering algorithms which adjust the defined clusters through numerous iterations until the results converge to a set of output clusters. However, BGMMs diverge from K-Means by inferring the ideal number of clusters to describe the input data, describing such clusters using Gaussians, and probabilistically assigning points to clusters, thus providing generally more robust clustering for data clouds where the clusters may be close together or overlapping, as is the case within the two main fracture zones activated in 2024. One issue with BGMM clustering and other machine learning clustering methods is a dependence on input order. To address this, random sorting of the event catalog is implemented, and the BGMM is run multiple times. After clusters have been identified, Principal Component Analysis is used to fit planes through the identified clusters and determine their degrees of planarity. Calculations are also run to determine the strike, dip, and area of the planes. The results from the multiple runs are assessed to determine the variability in clustering and to characterize the range of potential fracture planes defined by the microseismicity. For stages 3R through 10, we find 23 to 28 overlapping and en-echelon planes roughly in alignment with the SHmax determined from borehole breakouts at Utah FORGE.

1. INTRODUCTION

The Utah Frontier Observatory for Research in Geothermal Energy (Utah FORGE) is a field scale laboratory on the west flank of the Mineral Mountains outside Milford, Utah designed to study and help de-risk a geothermal technology known as Enhanced Geothermal Systems (EGS) (e.g. Moore et al., 2020, Moore et al., 2023). This form of geothermal technology does not require finding an underground reservoir of water like conventional geothermal but rather relies on finding hot rocks beneath the surface, drilling wells into them, and fracturing the rocks between the wells through a process known as stimulation. In stimulation, the wells are perforated along their side at several locations at depth, and then pressurized "water" (technically slick water and proppants – a special water solution and particles designed to create fractures and hold them open) is pumped through each of these openings at depth, starting with the one(s) at the bottom of the well, and moving up the well by temporarily blocking off the lower one(s). Each phase of openings in the well that is stimulated is known as a stage. This whole process can generate microseismic activity (i.e. tiny earthquakes) when pressurized water creates and flows through fractures in the rock.

Careful monitoring and understanding of seismicity in an EGS system is one of the essential goals of the Utah FORGE project (e.g. Moore et al., 2020, Moore et al., 2023, Pankow et al., 2025, Niemz et al., 2024a), as past endeavors in EGS have ended very poorly, e.g., Pohang, South Korea (Ellsworth et al., 2019). One important aspect of understanding the seismicity associated with EGS is understanding the creation and propagation of fractures within the geothermal reservoir. With this, it is important to know whether the fractures being activated are new, are the same ones created in previous phases of stimulation, or are a reactivation of pre-existing faults. Studying the fractures over time can possibly show whether the fractures are linking to each other in the way intended for the reservoir, or whether they are expanding toward a larger fault system in the area, potentially leading to increased seismic hazard.

In April 2024, the injection well at Utah FORGE was stimulated in eight stages (Stages 3R, 4, 5, 6 a and b, 7, 8, 9, and 10). This stimulation process generated a corresponding microseismic catalog of 2,900 events (Niemz et al., 2025) (Figure 1). In this study, we use this catalog to cluster microseismicity, identify fracture planes, and determine properties of the planes, such as strike, dip, planarity, and area.

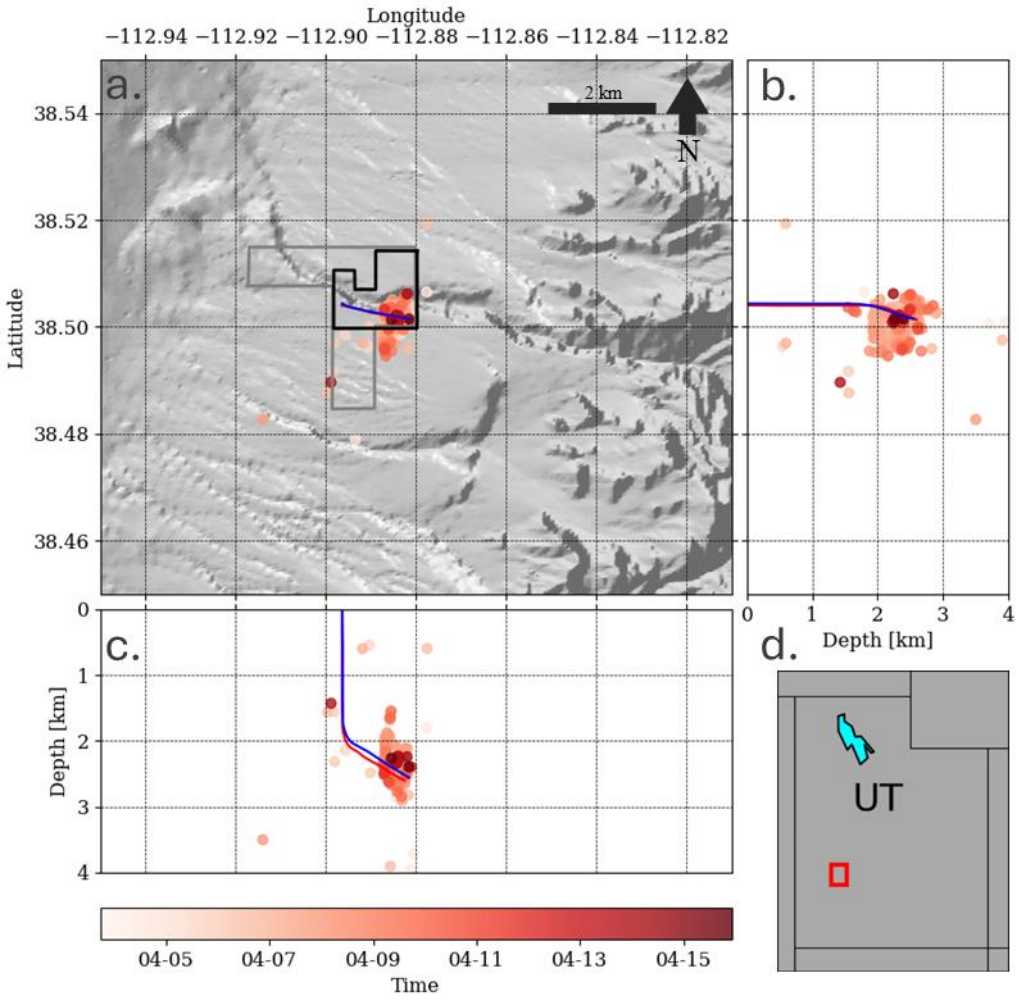

Figure 1: (a) Map of the Utah FORGE site, with the current site boundary outlined in black, the original boundary in dark gray, traces for wells 16A and 16B in red and blue, respectively, and the Niemz et al. (2025) microseismic catalog used for this study as red circles, shaded by time during the stimulation. (b) North-South cross-section of the microseismicity. (c) East-West cross-section of the microseismicity. (d) Location of the Utah FORGE site within the State of Utah indicated by a red box.

2. DATA & METHODS

For this study, we use the Niemz et al. (2025) microseismic catalog from the 2024 stimulation at Utah FORGE. (Figure. 1) The key finding from Niemz et al. (2025) is that microseismicity falls into two main fracture zones. The microseismic catalog from that study is derived from five permanent surface stations surrounding the Utah FORGE site, as well as a temporary deployment of 144 nodal geophones deployed during the stimulation. The microseismic catalog contains 2,900 events (M_L -1 to 2.03) which underwent relative relocation.

In order to determine the fracture planes illuminated by microseismicity, we started from a workflow developed in Karvounis et al. (2023), which uses a Bayesian Gaussian Mixture Model (BGMM) to group or 'cluster' events and then Principal Component Analysis (PCA) to flatten the clusters into two dimensions, allowing for visualization of the likely fracture planes. BGMMs are similar to the more popular K-Means clustering method in that both are unsupervised clustering algorithms which adjust the defined clusters through numerous iterations until the results converge to a set of output clusters. However, whereas for K-Means, the user must specify the desired number of clusters, BGMMs diverge by inferring the ideal number of clusters to describe the input data, describing such clusters using Gaussians, and probabilistically assigning points to clusters, thus providing generally more robust clustering for data clouds where the clusters may be close together or overlapping, as is the case within the two main fracture zones activated in 2024. We use only the spatial parameters of the microseismic events (x - position in meters east of the wellhead, y - position in meters north of the wellhead, and z - depth in meters from the surface) for consideration in the clustering algorithm, first normalizing the values of each parameter, so no one spatial parameter would have an oversized impact on the clustering.

When the model is run, it takes the input data and picks a few starting points to build clusters, called initialization points. From these, it iterates over the data points until all are separated into clusters, continually updating the clusters until they have reached an internally-set convergence tolerance that defines how precise the model ought to be in defining that the clusters have converged to a viable solution. It then picks new initialization conditions and runs again, doing this a pre-specified number of times, ultimately outputting only the best-fitting result from these multiple runs. Within the BGMM algorithm, there are many controls that can be adjusted to change how the model functions. We set the maximum number of Gaussian clusters the model can use each time to 75, which was more clusters than the model tried using, even when tested on a much larger dataset. We set the maximum number of iterations allowed for the model to try converging to 5,000. We tested the convergence tolerance of the model by setting the threshold for convergence to 10^{-3}, 10^{-4}, 10^{-6}, 10^{-8}, and 10^{-10}, and found no meaningful change in the output results above 10^{-4}, so we elected to proceed with 10^{-6}. We specified that the model should allow each cluster to possess its own covariance matrix, meaning that every cluster can have its own shape, rotation, and orientation, which is the most flexible option for the model. We set the model to follow a Dirichlet Process, allowing it to infer from the data the best number of clusters to use, applying a mean precision parameter of 0.8 to limit overfitting the data, while also ensuring that the model positions the clusters based on the data instead of biasing their positions toward an arbitrary position vector. We define the initialization process to utilize K-Means, thus letting the model apply an educated guess to determine the starting points from which to build the clusters. Importantly, to ensure reproducibility between runs, we fix the random state parameter to 100, which controls all randomness within how the model runs, including the starting point of the K-Means process underpinning the BGMM's initializations. We then tell the model to run the entire process, initialization selection and all, five times over every time we run the model, outputting to us the best result from the five runs.

The next step is to perform Principal Component Analysis (e.g. Michelini & Bolt, 1986, Shearer & Hardebeck, 2003). Evaluating only clusters which contain at least five microseismic events, we can infer that the clusters of seismicity are three-dimensional (3D) shapes. Therefore, we use PCA to determine the smallest dimension of each cluster, and flatten it to zero, thereby leaving us with a two-dimensional (2D) shape that mimics the fracture plane the seismicity most likely occurred along. However, just because one dimension of a cluster is smallest does not necessarily imply that the cluster actually represents a plane. Therefore, we compute the eigenvectors that describe the orientation of each cluster, and then compute the planarity of each cluster using Equation 1 (Gammans, 2013):

$$\text{Planarity} = 1 - \frac{2*\lambda_3}{\lambda_1+\lambda_2} \tag{1}$$

where λ_1 is the principal (or largest) component vector – typically in the strike direction of a fracture plane, λ_2 is the second principal (or second largest) component vector – typically in the dip direction of a fracture plane, and λ_3 is the third principal (or smallest) component vector – typically the in the width direction of a fracture plane. The λ_3 direction is often assumed to be zero for the idealized model of a fracture plane, hence why we use PCA to reduce this component to zero. Using equation (1), we confirm that all clusters output by the BGMM adhere to a planarity greater than or equal to 0.9, labeling any below that value as outliers. We then compute the plunge and trend of the poles of each of these planes to more easily describe their orientations. To help with visualization of the planes in 3D space and compute their approximate areas, we define rectangular planes that span the region covered by the events within each cluster. These planes are defined by taking the two furthest apart events in each of the first two principal directions, computing the average distance from the center of the cluster to the event for each of these two point pairs, which we call the half-length and half-width of the planes, multiplied by a small padding factor to help with the visual fit of the planes. We can then use combinations of the half-length and half-width summed or subtracted from the coordinates of the planes' centers to obtain the coordinates of the corners for each plane, which can then be plotted for clear visualization. To compute the area of the planes, we split each plane into two triangles along a shared diagonal, for each triangle computing half the magnitude of the cross product of an edge vector and the diagonal, summed with half the cross product of the other edge vector and the same diagonal. This yields an accurate computation for the area of our planes that would work beyond our exclusively rectangular planes, no matter their quadrilateral shape.

We note that the BGMM has a subtle dependence on the input order of the microseismic data for the K-Means initialization process. To remove the effect of potential time-biasing from our chronological event catalog, we introduced randomization of the row order in our catalog before processing with the BGMM and PCA and ran through 100 such randomizations, obtaining output clusters and planes from each of these runs. This shuffling of our input catalog acts similar to changing the random state parameter in our BGMM, by adjusting which data points are selected as initialization points for the clustering algorithm. However, as the random state parameter also controls other randomness factors in the BGMM, we seek to "control" the randomness by only changing one factor – the initialization points – thereby allowing for consistent comparison of the results, while also maintaining reproducibility in the model. After performing runs of the machine learning algorithm with 100 randomizations of the input dataset's row-ordering, we found that all runs sorted the data into 23 to 28 clusters with the most by far containing 27 clusters (Figure 2). To quantify whether the clusters defined by the 100 runs are the same or different planes, we plotted the centers of all the planes defined across the runs. We took the most common number of clusters and performed K-Means clustering, setting the k parameter – which defines the number of desired clusters – to the most commonly-obtained result; in this case, 27. From these clusters, we ran statistics on the parameters describing the planes the points in these clusters represent, finding the minimum, maximum, mean, median, mode, and standard deviation of the x-position (easting), y-position (northing), z-position (depth), event count, planarity, area, and plunge and trend of the pole to each plane. The orientations of the mean planes for each of these six clusters were then plotted on a Stereonet for visualization. Establishing this workflow has allowed for analysis of the fracture planes activated at Utah FORGE during the April 2024 stimulations.

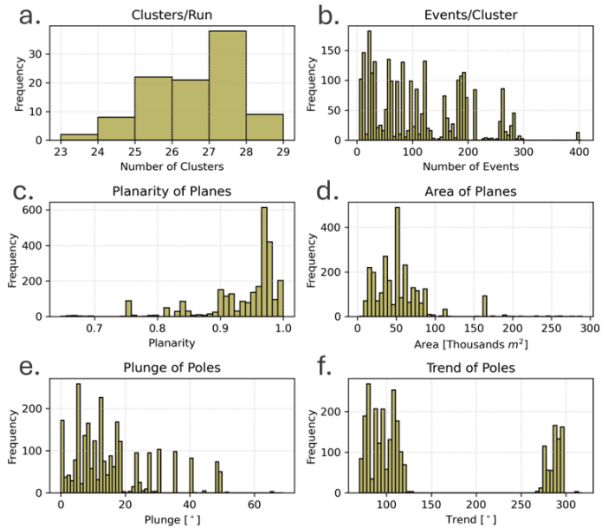

Figure 2: The six panels show histogram results of clustering runs for 100 randomizations of the input catalog of 2,900 events. (a) number of clusters obtained per run (2,612 total), (b) number of events grouped into each cluster, (c) planarity of the cluster planes defined, (d) approximate area of the cluster planes in meters squared, (e) plunge of the poles for each cluster plane, and (f) trend of the poles for each cluster planes.

3. RESULTS

From the 100 runs of the clustering algorithm, 2,612 different clusters describing planes were defined (Figure 2). From each run of the BGMM clustering algorithm, a fairly consistent number of clusters resulted with each run giving 23 to 28 clusters, though 27 was by far the most common as seen in Figure 2 (a). These planes were defined by a broad range in quantities of microseismic events per plane, though peaks can be seen in Figure 2 (b) around 25, 75, 125, 190, and 275 events. Of the 2,612 planes defined, 2,128 planes fit the criteria of a planarity greater than or equal to the 0.9 threshold, meaning 484 planes were not planar and were excluded from future analysis. The range of areas computed for the planes span from 2,800 m^2 to 290,000 m^2, though the vast majority fall between 5,000 m^2 and 100,000 m^2. This may be indicative of the same planes forming reliably from the clustering across the 100 runs. Of note is that the x-axes on the plunge and trend panels in FIG 2 are not scaled to the full range of 0 – 90° plunge, and 0 – 360° trend. Instead, the poles of the planes are fairly tightly oriented, especially in their trend, with the plunge of the poles mainly ranging 0 – 50° and the trend falling into two groups, between ~90 – 120° and ~270 – 300°. Continuing beyond this initial analysis of the resultant planes, we noticed that the centers of the planes (defined in x-y-z coordinates as the center of the rectangular planes) grouped into a few key positions (Figure 3).

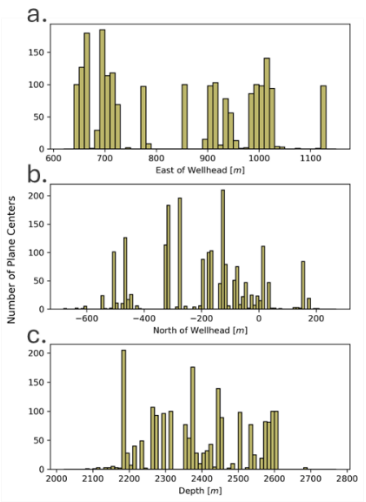

Figure 3: The three panels show cross-sectional histograms for the positions of the plane centers in (a) X – distance east of the wellhead in meters, (b) Y – distance north of the wellhead in meters (negative indicating south), and (c) Z – depth beneath the surface in meters.

From the east position, four distinct groups of centers appear around 650 m, 700 m, 900 m, and 1000 m. The north positions group into a few distinct localities, with two large histogram bars around -300 m, another around -160 m, and a few smaller ones around -500 m, -200 m, and 0 m. The depth regions are slightly more uniformly distributed, though with a few notable spikes around 2,180 m, 2,380 m, and 2,450 m. After seeing these distinct positions appear in a large majority of the 100 runs, we clustered the positions of the plane centers using K-Means, with the model's k-value – the parameter defining the number of clusters to use – set to the most common number of clusters output by the BGMM, in this case, 27. The results of this clustering can be seen in Figure 4. The fact that many of the 2,128 centers overlay each other is predominantly not a matter of visualization, but rather is a product of the plane centers obtained from the 100 runs of the BGMM algorithm possessing the same positions in a consistent fashion. This allows for greater confidence to be had in the algorithm's quantitative ability to describe the fracture planes in Utah FORGE's geothermal reservoir. As shown in Figure 5 and Table 1, many of the planes all share roughly the same orientations, despite locating to different areas within the reservoir.

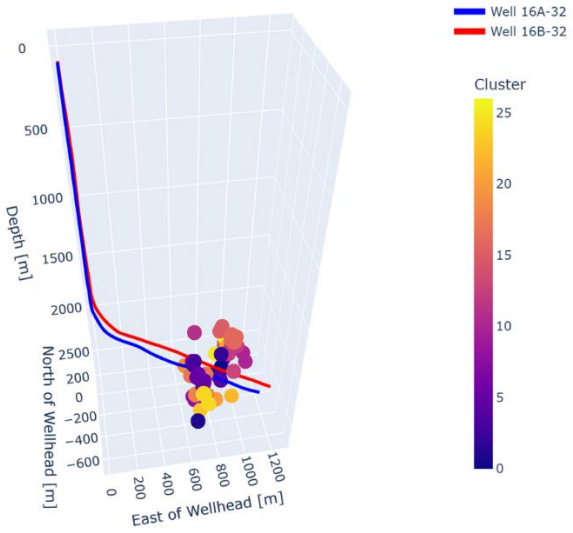

Figure 4: 3D plot, showing how the centers of the 2,128 planes locate in space in relation to wells 16A and 16B and group into 27 clusters. Note: there are 2,128 points on this plot, but many share the exact same position, and the points therefore overlay each other.

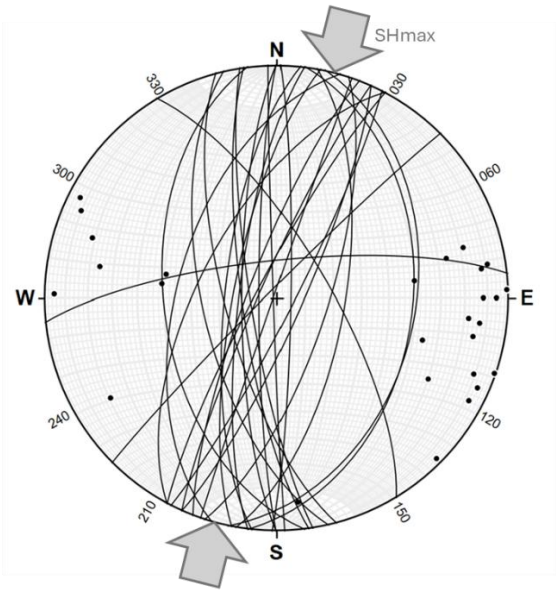

Figure 5: Stereonet of the mean poles and planes from the clustering of the centers of the planes from the 100 runs.

Table 1: Results from the clustering of the plane centers shown in Figures 4 and 5. Data represented as the means ± 1 standard deviation. Note: significant figures are rounded to the nearest meter and nearest degree so as not to over-interpret results since meter-plus-scale error is present in the microseismic catalog.

Cluster	X [m]	Y [m]	Z [m]	Event Count	Plunge [°]	Trend [°]
0	939 ± 7	-68 ± 16	2583 ± 19	288 ± 61	5 ± 2	271 ± 60
1	644 ± 0	-697 ± 1	2314 ± 1	260 ± 2	9 ± 0	81 ± 0
2	915 ± 0	-176 ± 0	2261 ± 0	183 ± 1	13 ± 0	97 ± 0
3	694 ± 2	-272 ± 2	2187 ± 6	190 ± 14	6 ± 2	90 ± 1
4	904 ± 1	-201 ± 5	2502 ± 1	193 ± 12	12 ± 2	82 ± 2
5	722 ± 10	-471 ± 14	2184 ± 18	21 ± 3	24 ± 1	280 ± 23
6	981 ± 0	14 ± 1	2534 ± 5	124 ± 13	7 ± 1	118 ± 1
7	705 ± 0	-122 ± 1	2372 ± 1	82 ± 1	18 ± 1	75 ± 1
8	659 ± 4	-462 ± 11	2375 ± 5	100 ± 12	49 ± 0	277 ± 1
9	777 ± 1	-326 ± 3	2595 ± 0	55 ± 1	6 ± 1	297 ± 0
10	1123 ± 1	-126 ± 7	2441 ± 3	6 ± 0	35 ± 4	106 ± 2
11	711 ± 0	-167 ± 1	1997 ± 0	121 ± 1	1 ± 0	88 ± 0
12	1016 ± 11	-37 ± 10	2401 ± 17	136 ± 35	6 ± 6	114 ± 22
13	992 ± 0	-274 ± 1	2359 ± 1	191 ± 2	18 ± 1	96 ± 0
14	1020 ± 3	163 ± 8	2566 ± 10	65 ± 12	1 ± 2	109 ± 0
15	947 ± 5	34 ± 7	2238 ± 1	12 ± 0	27 ± 3	118 ± 1
16	1019 ± 11	-107 ± 22	2198 ± 16	35 ± 8	26 ± 2	77 ± 2
17	665 ± 28	-312 ± 13	2295 ± 18	68 ± 13	15 ± 3	101 ± 42
18	661 ± 8	-506 ± 4	2271 ± 2	96 ± 7	10 ± 0	111 ± 17
19	691 ± 11	-114 ± 22	2461 ± 9	31 ± 3	40 ± 6	83 ± 7
20	854 ± 0	-320 ± 0	2605 ± 1	59 ± 1	18 ± 1	288 ± 0
21	1009 ± 4	5 ± 13	2435 ± 11	222 ± 46	13 ± 2	174 ± 92
22	946 ± 0	-426 ± 0	2446 ± 0	77 ± 0	12 ± 0	90 ± 0
23	691 ± 5	-537 ± 14	2409 ± 2	28 ± 2	50 ± 1	282 ± 4
24	701 ± 10	-627 ± 31	2139 ± 18	30 ± 6	18 ± 7	239 ± 69
25	899 ± 0	-53 ± 0	2390 ± 0	159 ± 1	9 ± 0	294 ± 0
26	1025 ± 7	150 ± 26	2449 ± 12	61 ± 14	3 ± 2	135 ± 67

4. CONCLUSION

The numerous runs of the machine learning workflow present encouraging results showing the rigorous nature of the workflow that has been created. Reliably obtaining 23 to 28 similar clusters from repeated runs of the algorithm, with cluster center that themselves group spatially, provides confidence that our quantitative analysis is robustly describing fracture planes present at Utah FORGE from stages 3R through 10 of the April 2024 stimulation. As can be seen by combining the views from the three panels of Figure 6 with the stereogram in Figure 5, the fractures not only line up with similar orientations, but appear to form a system of overlapping, en-echelon fractures that align decently well with SHmax – the orientation perpendicular to the least compressive stress direction – as well as fault plane orientations reported by Rutledge et al. (2025). The next step for this study is to expand the analysis to the microseismic catalogs for the 2022 stimulation and the 2023 circulation to see if fracture development can be determined for stage 3 of injection.

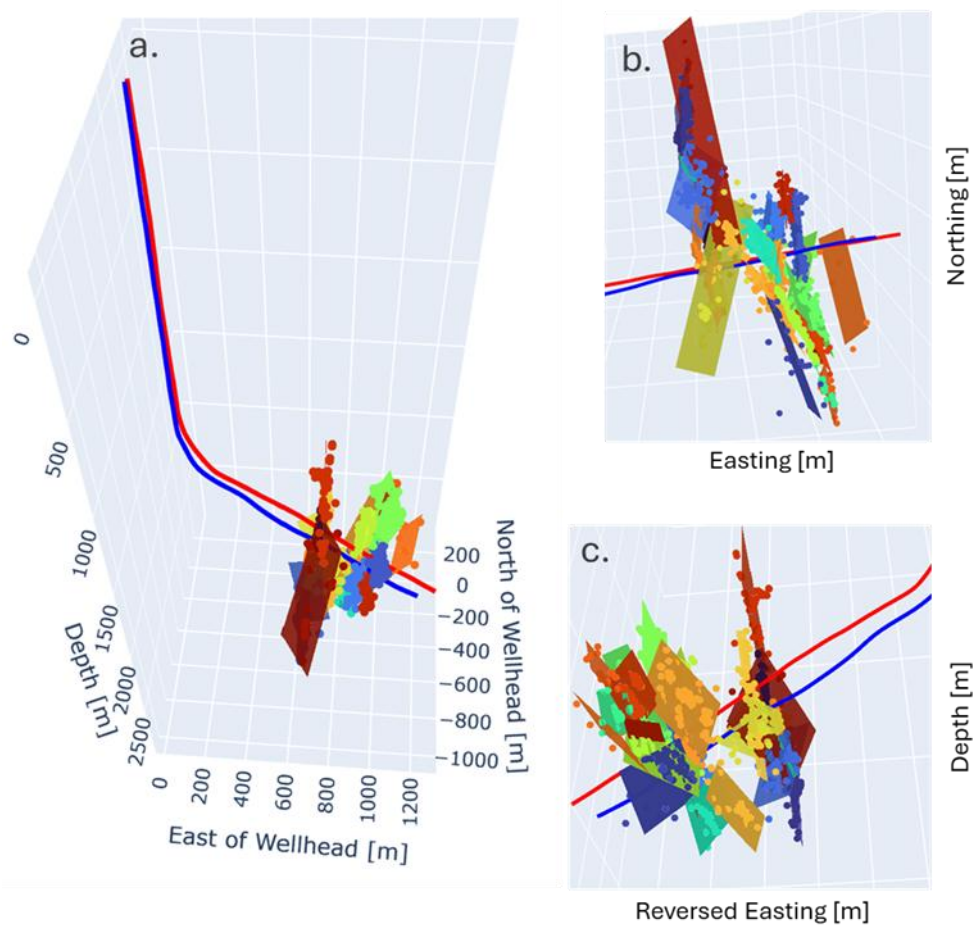

Figure 6: 3D view of the modeled planes. The planes visualized here are not the mean planes, but a representative example from a single of the 100 runs. (a) A full 3D view of wells 16A and 16B, red and blue, respectively, with modeled planes and the microseismic events corresponding to each plane in matching colors, (b) a view from below of the same planes as in (a) with North downward, East toward the right, and depth decreasing into the image, and (c) a zoomed-in view from the opposite direction as in (a), with depth decreasing downward, East toward the left, and North pointed out of the image.

5. ACKNOWLEDGEMENTS

Thanks to Dr. Peter Lippert for reviewing an earlier manuscript. Funding for this work was provided by the U.S. DOE under grant DE-EE0007080 "Enhanced Geothermal System Concept Testing and Development at the Milford City, Utah FORGE Site." and by the Swiss Federal Office of Energy within the framework of the subsidy contract for the Haute Sorne project (contract MF_021-GEO-ERK). We thank the many stakeholders supporting this project, including the University of Utah, Smithfield, Utah School and Institutional Trust Lands Administration (SITLA), Beaver County, and the Utah Governor's Office of Energy Development.

REFERENCES

Ellsworth, W. L., Giardini, D., Townend, J., Ge, S., & Shimamoto, T. (2019). Triggering of the Pohang, Korea, Earthquake (M_w 5.5) by Enhanced Geothermal System Stimulation. *Seismological Research Letters*, *90*(5), 1844–1858. https://doi.org/10.1785/0220190102.

Gammans, C. N. (2013). Low-angle Normal Faulting in the Basin and Range – Colorado Plateau Transition Zone During the January 3, 2011 Circleville, UT Earthquake Sequence. (Master's Thesis). University of Utah, Salt Lake City, Utah, https://collections.lib.utah.edu/details?id=196091.

Karvounis, D., Castilla, R. C., Meier, P., Kristjánsdóttir, S., Ritz, V., Rinaldi, A. P., Hjörleifsdóttir, V., & COSEISMIQ Team (2023). Calibration of a high enthalpy geothermal reservoir model utilizing micro-seismicity data. *Proceedings, World Geothermal Congress 2023*, Beijing, China, 12p.

Moore, J., McLennan, J., Pankow, K. L., Finnila, A., Dyer, B., Karvounis, D., Bethmann, F., Podgorney, R., Rutledge, J., Meir, P., et al. (2023). Current activities at the Utah Frontier observatory for research in geothermal energy (FORGE): A laboratory for

characterizing, creating and sustaining enhanced geothermal systems, *Proceedings, 57st US Rock Mechanics/Geomechanics Symposium*, Atlanta, Georgia, ARMA, ARMA-2023-0749 pp.

Moore, J., McLennan, J., Pankow, K. L., Simmons, S., Podgorney, R., Wannamaker, P., Rickard, W., & Xing, P. (2020). The Utah Frontier Observatory for Research in Geothermal Energy (FORGE): A laboratory for characterizing, creating and sustaining enhanced geothermal systems, *Proceedings, 45th Workshop on Geothermal Reservoir Engineering*, Stanford University, Stanford, California, SGP-TR-216 pp.

Michelini, A., & Bolt, B., A. (1986). Application of the principal parameter method to the 1983 Coalinga, California, aftershock sequence, *Bulletin of the Seismological Society of America*, *76*, 409–420.

Niemz, P., McLennan, J., Pankow, K. L., Rutledge, J., & England, K. (2024a). Circulation experiments at Utah FORGE: Near-surface seismic monitoring reveals fracture growth after shut-in. *Geothermics*, *119*, 102947. https://doi.org/10.1016/j.geothermics.2024.102947.

Niemz, P., Pankow, K. L., Isken, M., Whidden, K., McLennan, J., & Moore J. (2024b). Utah FORGE 2024 stimulations: Microseismic event catalog from seismic surface network. https://doi.org/10.5281/zenodo.12817880.

Niemz, P., Pankow, K. L., Isken, M. P., Whidden, K., McLennan, J., & Moore, J. (2025). Mapping fracture zones with nodal geophone patches: Insights from induced microseismicity during the 2024 stimulations at Utah FORGE. *Seismological Research Letters*, *96*(3), 1603-1618. https://doi.org/10.1785/0220240300.

Pankow, K. L., Dyer, B., Rutledge, J., Karvounis, D., Niemz, P., Whidden, K., Meier, P., Jaques, P., Petersen, G., Eaton, D., Shemeta, J., & Moore, J. (2025). Lessons from Utah FORGE for Seismic Monitoring of Engineered Geothermal Systems. *Proceedings, 50th Workshop on Geothermal Reservoir Engineering*, Stanford University, Stanford, CA, Feb. 10-12, 15p.

Rutledge, J., Pankow, K. L., Niemz, P., Dyer, B., & Karvounis, D. (2025). Microseismic source mechanisms during a Utah FORGE injection stimulation. *Proceedings, 50th Workshop on Geothermal Reservoir Engineering*, Stanford University, Stanford, CA, Feb. 10-12, 8p.

Shearer, P. M., & Hardebeck, J. L. (2003). Analysis of similar event clusters in aftershocks of the 1994 Northridge, California, earthquake, *Journal of Geophysical Research*, *108*(B1), 2035, doi:10.1029/2001JB000685.